Journal of Robotics and Control (JRC)
Volume 6, Issue 1, 2025
ISSN: 2715-5072, DOI: 10.18196/jrc.v6i1.24411

Analysis of Design Considerations for a 6 DoF Mobile Manipulator Based on Manipulability Measure

Shyju Susan Mathew [1*], Jisha V R [2]
[1] Research Scholar, Department of Electrical Engineering,College of Engineering Trivandrum
Assistant Professor, Mar Baselios College of Engineering and Technology, India
[2] Professor, Department of Electrical Engineering,College of Engineering Trivandrum, India
APJ Abdul Kalam Technological University
Email: [1] shyju.mathew@mbcet.ac.in, [2] jishavr@cet.ac.in
*Corresponding Author

***Abstract*—Mobile manipulators are highly versatile and are used across various fields due to their flexibility, reach, and adaptability. Hence it finds applications that involve complex environments or require high precision. The mobile manipulation tasks require the manipulators to retain good manipulation capability, which calls for reasonable motion planning. Manipulability, a crucial metric indicating the robot's ability to perform effective and efficient manipulation tasks, serves as the central criterion for the design of redundant mobile manipulators (MM). In addition to this, for applications where the mobile base and manipulator are moving simultaneously, a design configuration with good manipulability measure is preferred. This study fills a significant gap in the literature by offering an analysis of the design considerations for a redundant MM for improved manipulability measure. In this paper, the end effector of a 6 DoF MM is made to move through a predefined trajectory, and the manipulability measure and manipulability ellipsoid are computed at various points in the workspace. The analysis is done based on various link length ratios, mounting positions of the arm, and mobile base speeds. The manipulability ellipsoids at various locations in the task space were analyzed which is indicative of maximum and minimum velocities achievable by the end effector. Based on the analysis, the best configuration is identified and a kinematic controller is designed for this configuration which traces the reference trajectory with high manipulability. An exhaustive simulation study shows the benefits of the suggested design principles and control techniques, reaffirming the significance of optimized link lengths, mounting positions, and mobile base speeds in enhancing manipulability. Although this study is carried out in a 6 DoF MM, the novelty of this research lies in its emphasis on enabling design of redundant MM for better manipulability which lays a strong foundation for future applications.**

***Keywords*—Mobile Manipulator; Kinematics; Modeling; Manipulability; Manipulability Ellipsoid**

I. Introduction

A mobile base with a typical robotic arm makes up a Mobile Manipulator (MM) system. These MMs are frequently utilized for various tasks, including exploration, hauling big loads, neutralizing explosives, and maintenance in hazardous situations [1]–[4]. These significant applications have sparked a lot of interest in MM system research. Such robots are suitable for applications that require mobility and manipulation skills because they combine the benefits of greater manipulator dexterity and the vast workspace capacity of the mobile platform. A lot of progress has been made in the field of motion planning for mobile manipulators. The fundamental research approach is to create various performance criteria and then use them to identify the best solution for robotic kinematics. Most of the MMs employed in industrial applications possess kinematic redundancy. As these manipulators are kinematically redundant, in order to optimize the performance, many performance measures are considered. Manipulability Measure, Redundancy Index (RI), Condition Number of the Jacobian, Singularity Robustness etc are some of the indices used for performance analysis. The manipulability measure is crucial in analyzing mobile manipulators because it provides a quantitative assessment of how effectively and efficiently the manipulator can achieve desired movements or manipulate objects in its workspace. This is particularly important for mobile manipulators because they combine two key subsystems: the mobile base (which provides mobility) and the robotic arm (which performs manipulation tasks). Analyzing the manipulability of such a system helps to ensure that the robot can perform tasks with precision, avoid configurations where its performance is limited, and efficiently utilize its degrees of freedom. Hence manipulability measure is chosen as the performance criteria for the design of mobile manipulators [5]–[7].

In [8]–[11], motion planning of Mobile manipulators is done such that Manipulability Percentage Index or refined manipulability index is maximized. These formulations take MM's physical limitations also into account. Maximizing the manipulators' manipulability is proposed and studied as a solution to the problem of singularity that emerges in the plan-

ning and managing of a manipulator's movements. [12]–[16] discusses a motion planning method for tracking the kinematic trajectory of redundant non-holonomic MMs. Joint angle range, self-collision prevention, joint velocity restrictions, and joint velocity boundary restrictions are among the constraints taken into account. It presents a brand-new manipulability metric. The manipulabilities of the MM system and the manipulator arm are simultaneously improved by maximizing this new parameter. Operational Point-to-Point Tasks by MMs with 6DoFs are covered in [17]–[20]. Manipulability Percentage Index (MPI), a singularity avoidance indicator, is presented. In all the above-mentioned literature, even though the manipulability measure is considered as the performance measure for the design of the controller, none of them had done a detailed analysis of how the change in length ratio of the manipulator's arm affects the manipulability measure.

[21]–[24] create the practical base pose set for MMs and Capability Map (CM) based on manipulability values at each point in the workspace is developed. Generally, CM was built offline. The end effector poses and associated manipulation capability index are both stored. The best pose is one with the maximum manipulation potential without a collision is chosen. However, finding an optimal path for mobile robots from the capability map of large points is hard and time-consuming and hence CM with fewer points needs to be produced.

MM's manipulability was employed to resolve the operational motion planning issue for an MM with a 6 Dof arm in [25]–[28]. The relative weighting of manipulability measures is chosen based on the task. It combines the MM and the arm manipulability measure in a convex fashion. In [29]–[32] it is demonstrated that decreased velocity kinematics and velocity redundancy are suitable instruments to achieve operational tasks while maximizing criteria like manipulability. [33]–[37] considered both the manipulability and stability of the movable platform while examining the coordination between the manipulator and the platform. While these methods may effectively track the end-effector path while accounting for extra factors, none of them take into account how manipulator mounting position or length ratio affects manipulability and, consequently, reference trajectory tracking. [38]–[45] provided a solution based on optimization that can define the manipulator's intended joint configuration at the trajectory in addition to handling restrictions at the position level. In [46]–[49] the maximization of the manipulators' manipulability is considered as one of the performance criteria and it is essential to note that the manipulator's Jacobian matrix becomes rank deficient, and ill-conditioned when it is in a kinematic singularity configuration. This would cause the end-effector movement to fail in that direction. In reality, approaching the kinematic mapping's singularity point is similarly undesirable, if not unacceptable. This is because, in such a state, joint accelerations and velocities can be arbitrarily high [50]–[52], which would harm the physical manipulator when the end-effector moves in particular directions. Therefore, when it comes to singularity avoidance, manipulators' capacity for manipulation has explicit value. For the posture estimation, a better iterative closest point approach is devised in [53]. Algorithms and other criteria are researched to help the robot choose and alter its stance to maximize its manipulability for a specific manipulation job. [54]–[57], describes a novel method for regulating the instantaneous velocity of a robot end-effector, to maximize manipulability while avoiding joint restrictions. It functions on redundant and non-redundant robots by introducing redundancy in the form of well-managed path deviation. In [58] for the manipulator's arm affixed to mobile platforms, a systematic, unified kinematic analysis is discussed. To demonstrate how manipulator mounting position impacts the system's overall mobility, scaled manipulability ellipses are employed.

Even though a couple of the articles mentioned above discuss the simultaneous movement of the movable base and the manipulator, design considerations for better manipulability measures are not analyzed in these papers. In the literature, different manipulability measures are considered for motion planning but none of them gives a detailed analysis of design consideration for the selection of a particular manipulability measure. None of the literature discusses how to determine the appropriate manipulability measure for a given manipulation task to improve performance. This paper addresses this notable gap in the existing literature by conducting a comprehensive analysis of design considerations of 6 DoF MM based on manipulability measures. This analysis is a key aspect of redundant MM design that directly impacts its motion planning capabilities. The organization of the paper is as follows. Information on the kinematic modeling of a 6-DOF MM is provided in Section II. The examination of design considerations based on manipulability measures is presented in Section III. Design patterns for controllers are found in Section IV. Section IV presents the simulation findings. The paper is concluded in Section V.

II. Kinematic Modeling of 6 DoF Mobile Manipulator

In many of the applications like object sorting, loading and unloading, material transportation, safety and monitoring, maintenance and inspection, mobile manipulators are used which has extended workspace than a fixed manipulator. Many a time, these MMs are redundant and a performance measure like manipulability is to be used for analyzing the performance. A 6 DoF MM which is redundant, is considered in this work and it features a robotic arm that has three revolute joints (R) arranged with a spherical workspace. It also has a differential drive base, normally made up of two wheels with separate controls for mobility. The schematic diagram of the model considered for this study is shown in Fig. 1.

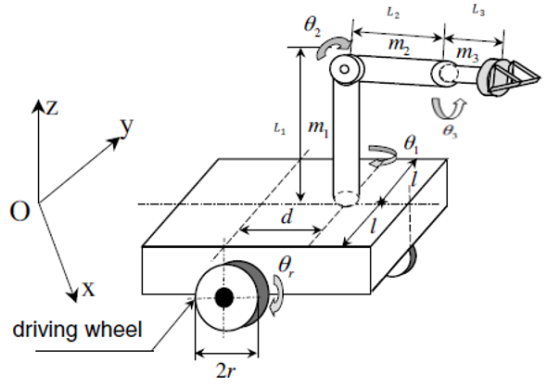

Fig. 1. 6-DOF MM on a movable platform with a manipulator on top [59]

A. Kinematic Model of Mobile Base

The mobile base of the MM with the differential drive is as shown in Fig. 2.

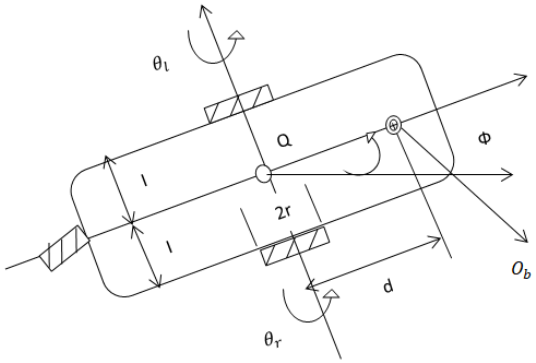

Fig. 2. Schematic diagram of a differentially driven mobile base

The center of gravity is assumed to coincide with the rotation point Q which is the midpoint of the two wheels. The specific mathematical terms utilized in the kinematic modeling are listed below:

- x_b, y_b indicates the position of the mobile base,
- ϕ is the mobile base orientation angle,
- θ_r, θ_l are the right and left wheel angles of the mobile base,
- $2l$ is the distance between the wheels and r is the radius of the wheel,

The kinematic equations of the wheeled mobile robot platform at the point O_b are:

$$\dot{x_b} = (\frac{r}{2}cos\phi + \frac{rd}{2l}sin\phi)\dot{\theta}_l + (\frac{r}{2}cos\phi - \frac{rd}{2l}sin\phi)\dot{\theta}_r \quad (1)$$

$$\dot{y_b} = (\frac{r}{2}sin\phi - \frac{rd}{2l}cos\phi)\dot{\theta}_l + (\frac{r}{2}sin\phi + \frac{rd}{2l}cos\phi)\dot{\theta}_r \quad (2)$$

$$\dot{\phi} = (\frac{r}{2l}(\dot{\theta}_l - \dot{\theta}_r) \quad (3)$$

The differential kinematics equation of the mobile base is:

$$\dot{p}_{base} = J_{base}\dot{q}_{base} \quad (4)$$

where

$$J_{base} = \begin{bmatrix} (\frac{r}{2}cos\phi + \frac{rd}{2a}sin\phi) & (\frac{r}{2}cos\phi - \frac{rd}{2a}sin\phi) \\ (\frac{r}{2}sin\phi - \frac{rd}{2a}cos\phi) & (\frac{r}{2}sin\phi + \frac{rd}{2a}cos\phi) \\ \frac{r}{2a} & -\frac{r}{2a} \end{bmatrix} \quad (5)$$

and

$$\dot{q}_{base} = \begin{bmatrix} \dot{\theta}_l \\ \dot{\theta}_r \end{bmatrix}, p_{base} = \begin{bmatrix} x_b & y_b & \phi \end{bmatrix} \quad (6)$$

J_{base} is the Jacobian matrix which relates the mobile base velocity with the wheel velocities and p_{base} is the position vector of the mobile base.

B. Kinematic Model of Manipulator

The location and orientation of the end-effector, which might be a gripper or a tool about the base frame, can be determined based on the kinematic model of an MM. In addition, it couples the velocities of the wheels to the linear and angular velocities of the movable base through the kinematics of the base. The manipulator parameters are listed below:

- θ_1, θ_2, θ_3 are the joint angles of the manipulator arm,
- L_1, L_2, L_3 are the link lengths of manipulator,
- d is the distance between the arm and the driving center of the mobile base.

To find the kinematic model of the manipulator, from the base to the end-effector of the 3R anthropomorphic robotic arm [59], frames must be allocated to each link to derive the forward kinematics. The transformation matrix from tool tip coordinates to base coordinates is:

$$T_0^3(\theta_1, \theta_2, \theta_3) = \begin{bmatrix} C_1C_{23} & -C_1S_{23} & S_1 & C_1(L_2C_2 + L_3C_{23}) \\ S_1C_{23} & -S_1S_{23} & -C_1 & S_1(L_2C_2 + L_3C_{23}) \\ S_{23} & C_{23} & 0 & L_1 + L_2S_2 + L_3S_{23} \\ 0 & 0 & 0 & 1 \end{bmatrix} \quad (7)$$

Hence the XYZ position of the end effector is obtained from the last column of $T_0^3(\theta_1, \theta_2, \theta_3)$.
The differential kinematics equation of the arm is:

$$\dot{p}_{arm} = J_{arm}\dot{q}_{arm} \quad (8)$$

where

$$q_{arm} = \begin{bmatrix} \theta_1 & \theta_2 & \theta_3 \end{bmatrix}^T$$

$$p_{arm} = \begin{bmatrix} x_{ee} & y_{ee} & z_{ee} \end{bmatrix}^T$$

J_{arm} is the arm Jacobian matrix with respect to the manipulator base frame. It gives the relationship between end effector velocity and joint velocities.

$$J_{11} = [-S_1(L_2C_2 + L_3C_{23})]$$

$$J_{12} = [C_1(-L_2S_2 - L_3S_{23})]$$

$$J_{21} = [C_1(L_2C_2 + L_3C_{23})]$$

$$J_{22} = [S_1(-L_2S_2 - L_3S_{23})]$$

$$J_{23} = [-S_1L_3S_{23})]$$

$$J_{31} = [0], J_{32} = [L_2C_2 + L_3C_{23}], J_{33} = [L_3C_{23}]$$

$$J_{arm} \begin{bmatrix} J_{11} & J_{12} & J_{13} \\ J_{21} & J_{22} & J_{23} \\ J_{31} & J_{32} & J_{33} \end{bmatrix} \quad (9)$$

The arm Jacobian matrix, $(\hat{J}_{arm})$ with respect to the mobile base frame when attached to the mobile base is:

$$\hat{J}_{arm} = R(\phi)J_{arm}S \quad (10)$$

where $R(\phi)$ is the rotation matrix about the world frame and S is the matrix that depicts the impact of mobile base velocity on arm velocity

$$R(\phi) = \begin{bmatrix} cos(\phi) & -sin(\phi) & 0 \\ sin(\phi) & cos(\phi) & 0 \\ 0 & 0 & 1 \end{bmatrix} \quad (11)$$

$$S = \begin{bmatrix} 1 - \frac{r}{2l} & \frac{r}{2l} & 1 \\ 0 & 1 & 0 \\ 0 & 0 & 1 \end{bmatrix} \quad (12)$$

C. Kinematic Model of Mobile Manipulator

The MM's wheel and joint velocities are related to the end effector velocity through the overall kinematic model. It has the following form and can be created by combining (5) and (10):

$$\begin{bmatrix} \dot{x_{ee}} \\ \dot{y_{ee}} \\ \dot{z_{ee}} \end{bmatrix} = J(q)\dot{q} \quad (13)$$

$$J(q) = \begin{bmatrix} J_{base} & \hat{J}_{arm} \end{bmatrix} \quad (14)$$

$$\dot{q} = \begin{bmatrix} \dot{q}_{base}^T & \dot{q}_{arm}^T \end{bmatrix} \quad (15)$$

$$\dot{q}_{base}(t)^T = \begin{bmatrix} \dot{\theta}_l & \dot{\theta}_r \end{bmatrix} \quad (16)$$

$$\dot{q}_{arm}^T = \begin{bmatrix} \dot{\theta}_1 & \dot{\theta}_2 & \dot{\theta}_3 \end{bmatrix} \quad (17)$$

$J(q)$ is the overall Jacobian of the MM. The MM's generalized coordinates are given in 18:

$$q = \begin{bmatrix} q_{arm}^T & q_{base}^T \end{bmatrix} \quad (18)$$

$q_{base} = [x_b, y_b, \phi]$: Platform configuration and $q_{arm} = [\theta_1, \theta_2, \theta_3]$: Manipulator configuration.

The 6 DoF MM which is considered in this work is a redundant manipulator and hence manipulability measure is an important factor that is to be considered in the design and analysis of such systems.

III. Manipulability Measure

The manipulability measure introduced by Yoshikawa [60] describes the ease with which an MM can arbitrarily adjust the position and orientation of the end-effector. It shows that a robotic system is capable of supplying end-effector speeds in either direction for a given design. It is an information about the dexterity and efficiency of the manipulator in performing various tasks. MMs often have redundant degrees of freedom, and the manipulability measure [61] provides insights into the redundancy of the manipulator and how it can be utilized to optimize the robot's motion. This redundancy can be exploited to improve performance, such as by achieving better manipulability in specific directions or avoiding joint limits. The entire set of end-effector velocities that can be achieved by joint velocities given by the equation (19):

$$\|\dot{q}\| = \sqrt{\dot{q_1}^2 + \dot{q_2}^2 + \dot{q_3}^2 + ... + \dot{q_n}^2} \leq 1 \quad (19)$$

is an ellipsoid which is called a manipulability ellipsoid in the m-dimensional Euclidean space, with m denoting the dimensionality of $\dot{X} = J\dot{q}$. The measurement is proportional to the manipulability ellipsoid's volume [62], [63]. The maximum speed of motion of the end effector is along the major axis and the minimum speed is along the minor axis of the ellipsoid. Fig. 3 displays the manipulability ellipsoid for various joint angles of the 6 DoF mobile manipulator arm with a specific link length ratio. According to the illustration, the manipulability ellipsoid changes as the joint angle changes.

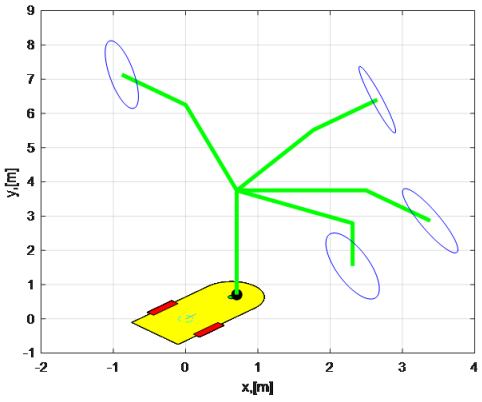

Fig. 3. Manipulability ellipsoid for different joint angles of the MM

This manipulability ellipsoid's physical significance is that [64], [65] the singular values offer the greatest end effector velocity that may be achieved by selecting joint velocity vectors from the set of all joint velocity vectors with a geometric norm of 1, which is defined by a unit sphere centered at the joint space origin. The greatest speeds that can be achieved in the various orthogonal directions of the task space are represented by distinct singular values. Although the minimal singular value is sometimes used as a broad indicator of manipulability, it is

frequently preferable to evaluate the system's manipulability in light of the task requirements.

The manipulability measure μ of the manipulator is defined as:

$$\mu = \sqrt{det(J(q)J(q)^T} \tag{20}$$

A. Quantitative Analysis of Manipulability Based on Different Design Considerations

Manipulability analysis is important in mechanical design and robotics, particularly when it comes to redundant mobile manipulators. For several reasons, including maximizing performance, covering workspace, task-specific design, avoiding singularities, and energy efficiency, manipulability analysis based on various design factors is crucial. Manipulability is influenced by several factors, including geometric designs, link length ratios, joint limits and base speeds, the mounting position of the arm on the base, etc. In this paper analysis of manipulability based on link different link length ratios, base speeds, and mounting positions are discussed.

1) Analysis of Manipulability Based on Link Length: Analysis of manipulability measures based on different link length ratios is essential for understanding how the geometry of a 6DoF MM affects its dexterity and workspace coverage. Also, it is essential to know about the maximum and minimum velocities that can be achieved in each direction which will help to analyze whether this configuration is suitable for an application. The link length ratio refers to the proportional lengths of the individual links in the manipulator's kinematic chain. Choosing a proper link length ratio is very important. The manipulability ellipsoid which is a graphical representation of the manipulability measure, provides valuable insights into the robot's kinematic capabilities. The major axis of the manipulability ellipsoid which is the longest one represents the direction in which the robot has the highest manipulability and can achieve the greatest motion in the workspace which means that the robot is more capable of achieving motion in that direction with relatively small changes in joint positions. It also implies that the robot can perform tasks with better precision and agility along this axis. The minor axis is the shortest axis of the manipulability ellipsoid. It represents the direction in which the robot has the lowest manipulability and can achieve the least motion in the workspace. Lower manipulability along this axis indicates that the robot has limited capability to reach certain positions or orientations in the workspace. This information is crucial for identifying potential limitations and understanding areas where the robot may struggle to perform certain tasks. If we choose a particular configuration (particular link length ratio), how well the manipulator is capable of performing a task in different directions is important. To analyze the same, testing is done with the given 6DoF mobile manipulator with different link length ratios. Table I shows the parameter values of the MM used for simulation.

TABLE I. PARAMETERS VALUES OF MOBILE MANIPULATOR

Symbol	Value	Unit
l_{ref}	0.6	m
Wheel radius(r)	0.2	m
Axle Length(2d)	1	m

Simulations are done by varying the link length ratios within a predefined range. A circular trajectory is considered for the end effector. These trajectories ensure smooth changes in velocity and acceleration leading to minimal abrupt forces or torques. Three different ratios of lengths have been considered. For each case, the manipulability ellipsoid's minor and major axes are found for different values of joint angles, and the results are compared. The link length ratios considered are:
A reference length of $l_{ref} = 0.6m$ is taken.
Case 1:$l_1 = 1.5l_{ref}$, $l_2 = 0.5l_{ref}$, $l_3 = 0.5l_{ref}$

For case 1, as in Fig. 4 and Fig. 5, the end effector trajectories are obtained and plotted for three different joint angle sets. The first and third joint angles are kept constant and the second joint angle varies over a range of 0 to 360 degrees. For each set, the major and minor axes of the manipulability ellipsoid are drawn which indicates the maximum and minimum motion achievable for the end effector.

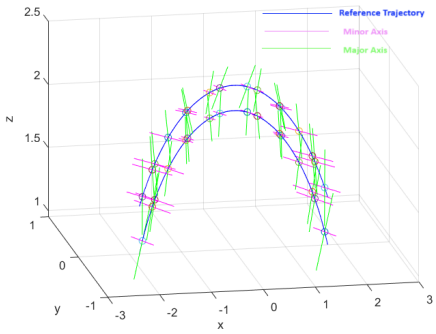

Fig. 4. Minimum and maximum velocities possible at different points on a reference trajectory in the required workspace - Link Length Ratio Case 1

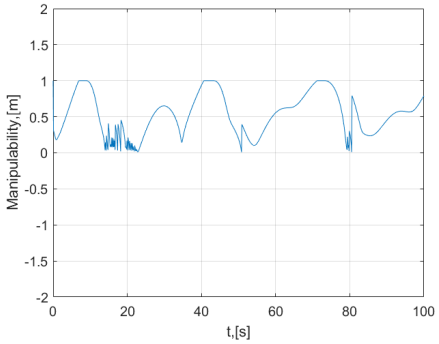

Fig. 5. Manipulability measures at the points considered on the reference trajectory for the first link length ratio - Case 1

For cases 2 and 3, as shown in Fig. 6 and Fig. 8, illustrate with the same joint angles but with different link length ratios.
Case 2:$l_1 = 1.5l_{ref}$, $l_2 = 1.5l_{ref}$, $l_3 = 1.5l_{ref}$

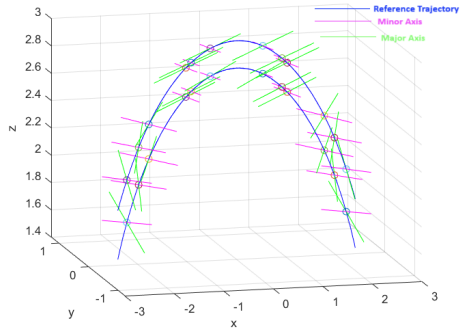

Fig. 6. Minimum and maximum velocities possible at different points on a reference trajectory in the required workspace for Link Length Ratio - Case 2

From Fig. 7 and Fig. 9, is can be seen that the manipulability is maintained at values between 0.5 and 1 throughout the operation and hence it is clear that the singularity is avoided during the entire operation.
Case 3:$l_1 = 1.5l_{ref}$, $l_2 = 1.0l_{ref}$, $l_3 = 1.0l_{ref}$

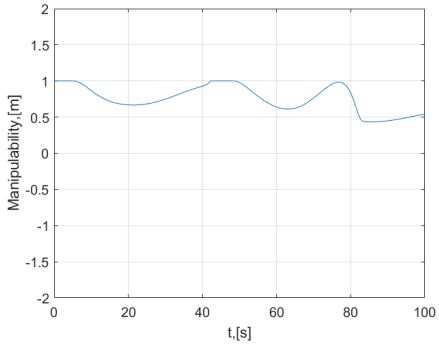

Fig. 7. Manipulability measures at the points considered on the reference trajectory for the first link length ratio- Case 2

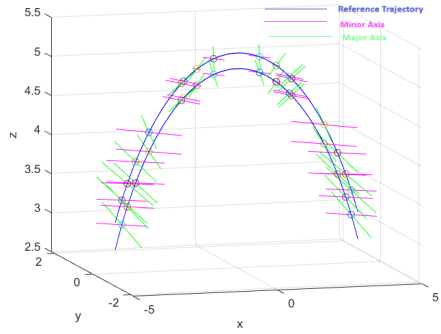

Fig. 8. Minimum and maximum velocities possible at different points on a reference trajectory in the required workspace for Link Length Ratio - Case 3

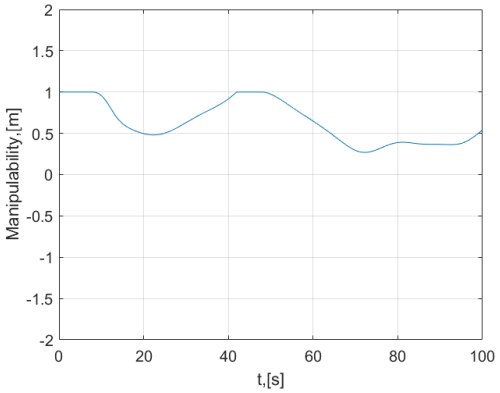

Fig. 9. Manipulability measures at the points considered on the reference trajectory for the first link length ratio Case 3

Tables II, III and IV show the minimum and maximum velocity ranges possible with the three cases of link length ratios. The multiplicity of different cases in these tables is due to similar points considered on either side of the circular trajectory.

Comparing the results for the three cases of link length ratios, it can be observed that link length ratio case 3 gives improved values for the minimum and maximum velocities possible at different points in the workspace and thus improved manipulability along different directions.

This is clear from Fig. 10 which shows that the elongation of the manipulability ellipsoid (which indicates the eccentricity of the manipulability ellipsoid) is less in case 3. This eccentricity quantifies the disparity between the lengths of the major and minor axes and indicates the difference between the manipulator's capabilities in different directions and hence indicates anisotropic manipulability.

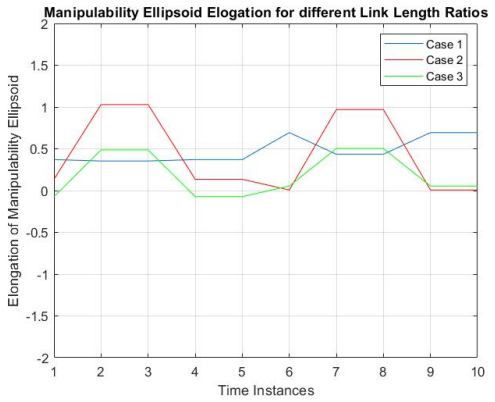

Fig. 10. Elongation of Manipulability ellipsoid for different link length ratios

The isotropic manipulability indicates that the manipulator has nearly equal capabilities in all directions, which is desirable for tasks requiring uniform performance Variation of manipulability for each case is also shown. Hence the link length

ratios significantly affect the manipulability of the MM. These findings can be used to optimize the manipulator's design for specific tasks and environments.

TABLE II. MINIMUM AND MAXIMUM VELOCITY RANGES POSSIBLE FOR LINK LENGTH RATIO - CASE 1

Maximum Range	Minimum Range
0.5403	0.1696
0.4293	0.0756
0.4293	0.0756
0.5403	0.1696
0.5403	0.1696
0.8689	0.1748
0.4984	0.0632
0.4984	0.0632
0.8689	0.1748
0.8689	0.1748

TABLE III. MINIMUM AND MAXIMUM VELOCITY RANGES POSSIBLE FOR LINK LENGTH RATIO CASE 2

Maximum Range	Minimum Range
0.6295	0.4942
1.1639	0.1350
1.1639	0.1350
0.6295	0.4942
0.6295	0.4942
0.5205	0.5135
1.1134	0.1441
1.1134	0.1441
0.5205	0.5135
0.5205	0.5135

TABLE IV. MINIMUM AND MAXIMUM VELOCITY RANGES POSSIBLE FOR LINK LENGTH RATIO CASE 3

Maximum Range	Minimum Range
0.2945	0.3669
0.6228	0.1359
0.6228	0.1359
0.2495	0.3669
0.2495	0.3669
0.4059	0.3519
0.6137	0.1104
0.6137	0.1104
0.4059	0.3519

B. Analysis of Manipulability Measure Based on Mounting Positions of the Arm

This analysis examines how the mounting position of the robotic arm affects its manipulability measure. Through this analysis, it is possible to identify optimal configurations for specific tasks and can help in designing workspaces and environments that maximize the utility of robotic arms. The analysis can also reveal situations where certain mounting positions may lead to singularities. As shown in (5), the Jacobian of the mobile base depends on the mounting position of the arm. Simulation is done for three different values for the mounting positions and the manipulability ellipsoids major and minor axes are illustrated in Fig. 11 to Fig. 16.

Case 1:Mounting position $d = 0.2m$

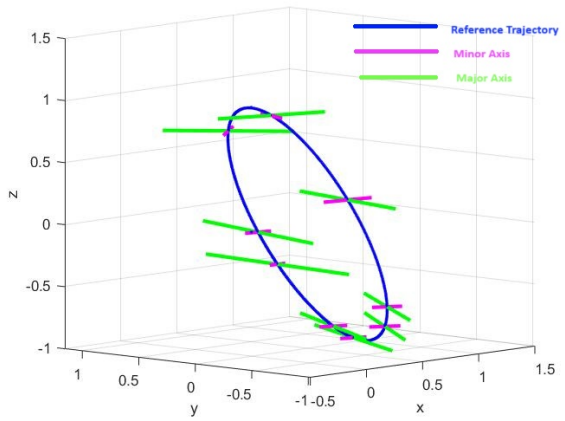

Fig. 11. Minimum and maximum velocities possible at different points along the reference trajectory for the mounting position $d = 0.2m$ -Case 1

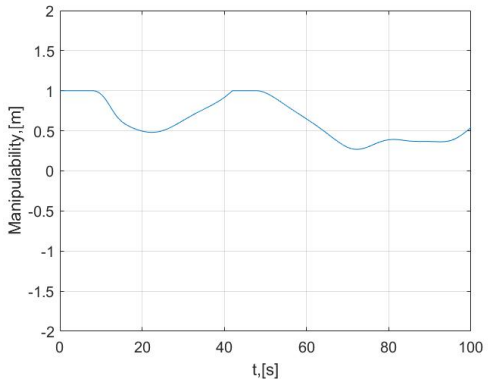

Fig. 12. Manipulability measures at the points considered along the reference trajectory for the mounting position $d = 0.2m$ - Case 1

Case 2:$d = 0.6m$

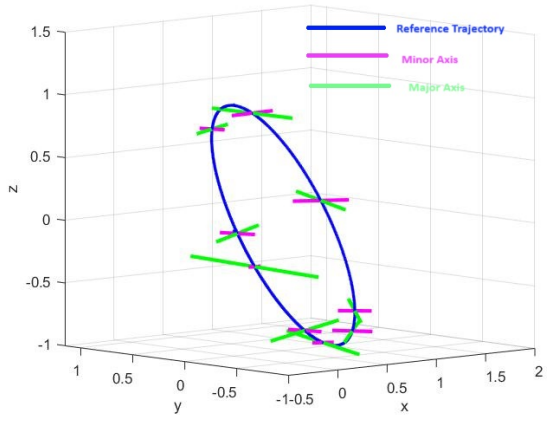

Fig. 13. Minimum and maximum velocities possible at different points along the reference trajectory for the mounting position $d = 0.6m$ - Case 2

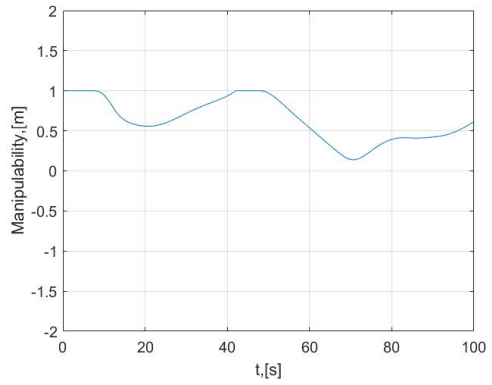

Fig. 14. Manipulability measures at the same points considered along the reference trajectory for the mounting position $d = 0.6m$ - Case 2

Case 3:$d = 0.8m$

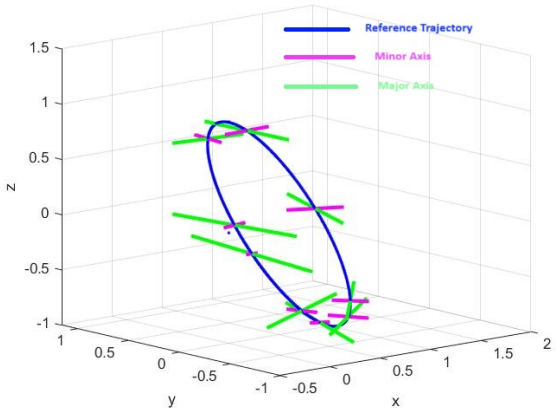

Fig. 15. Minimum and maximum velocities possible at different points along the reference trajectory for the mounting position $d = 0.8m$ - Case 3

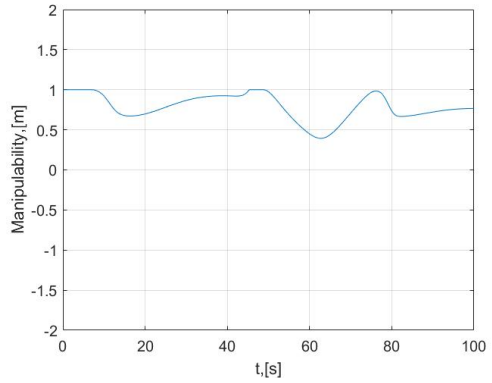

Fig. 16. Manipulability measures at the points considered along the reference trajectory for the mounting position $d = 0.8m$ - Case 3

Tables V, VI and VII tabulates the values of minimum and maximum possible ranges for velocity of the end effector for different mounting positions. Fig. 17 shows the elongation of the manipulability ellipsoid for the three cases of mounting positions. It is clear that case 3 mounting position with $d = 0.8m$ is giving better values for the minimum and maximum possible velocities which is represented by the minor and major axes of manipulability ellipsoid and thus better manipulability for the MM. For cases 1 and 2, only major axis values are high with low minor axis values, and therefore the set of possible end effector velocities are low which may finally lead to singularity.

TABLE V. MINIMUM AND MAXIMUM VELOCITY RANGES POSSIBLE FOR CASE 1 MOUNTING POSITION $d = 0.2m$

Maximum Range	Minimum Range
1.3904	0.1282
0.5745	0.1605
0.7540	0.1623
1.709	0.3532
0.6801	0.1275
0.4987	0.3673
0.3400	0.1836
0.6414	0.1629
0.7799	0.1642

TABLE VI. MINIMUM AND MAXIMUM VELOCITY RANGES POSSIBLE FOR CASE 2 MOUNTING POSITION $d = 0.6m$

Maximum Range	Minimum Range
0.1641	0.1110
0.5880	0.1459
0.9285	0.1736
0.4973	0.3663
0.747705	0.4335
0.5747	0.0732
0.9355	0.1161
1.2449	0.0968
1.0559	0.1756

TABLE VII. MINIMUM AND MAXIMUM VELOCITY RANGES POSSIBLE FOR CASE 3 MOUNTING POSITION $d = 0.8m$

Maximum Range	Minimum Range
0.1947	0.1033
0.5910	0.1354
0.9982	0.1761
0.4150	0.3985
0.812	0.4493
0.6315	0.0382
1.0695	0.2544
1.2410	0.0921
1.1245	0.1609

C. Analysis of Manipulability Measure Based on Different Base Speeds

The angular velocities of the wheels directly control the robot's motion. Manipulability depends on the robot's ability to perform these motions effectively. Changes in wheel angular velocities impact the robot's ability to translate and rotate simultaneously. Different wheel angular velocity profiles can affect the robot's ability to maneuver in dynamic environments.

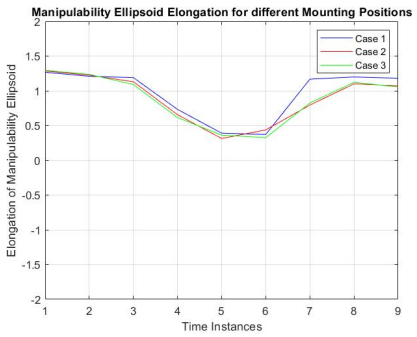

Fig. 17. Elongation of Manipulability ellipsoid for different mounting positions

The effect of different base speeds on manipulability is studied by conducting simulations for three different base speeds. The corresponding values of linear and angular velocities of the vehicle are as in Fig. 18 to Fig. 25 follows:

Case 1: $v = 0.2m/sec$, $\omega = 0rad/sec$

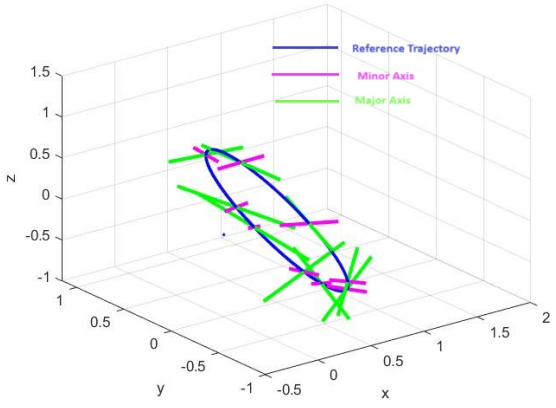

Fig. 18. Minimum and maximum velocities possible at different points along the reference trajectory for Base Speed $v = 0.2m/sec$

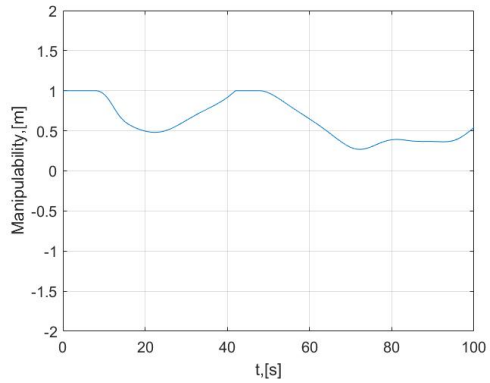

Fig. 19. Manipulability measures at the points considered along the reference trajectory for Base Speed $v = 0.2m/sec$

Case 2: $v = 1m/sec$, $\omega = 0.8rad/sec$

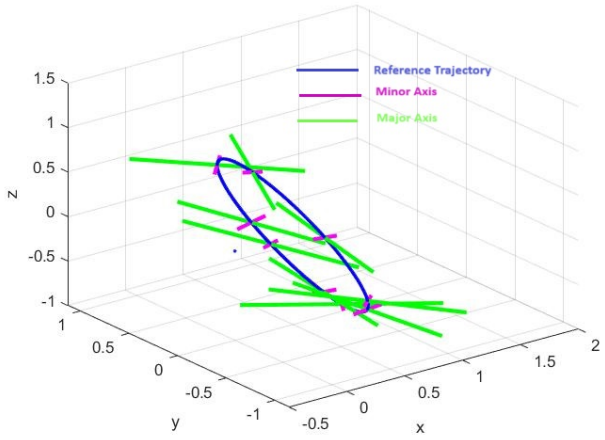

Fig. 20. Minimum and maximum velocities possible at different points along the reference trajectory for Base Speed $v = 1m/sec$

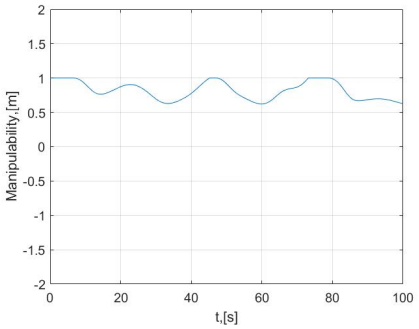

Fig. 21. Manipulability measures at the points considered along the reference trajectory for Base Speed $v = 0.4m/sec$

Case 3: $v = 2m/sec$, $\omega = 1.2rad/sec$

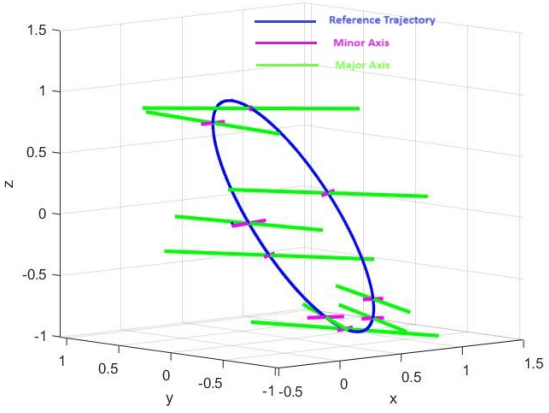

Fig. 22. Minimum and maximum velocities possible at different points along the reference trajectory for Base Speed $v = 2m/sec$

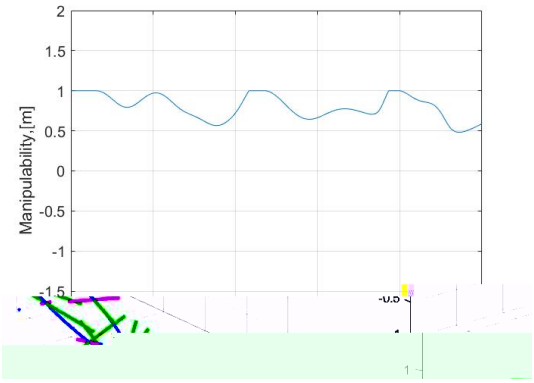

Fig. 23. Manipulability measures at the points considered along the reference trajectory for Base Speed $v = 2m/sec$

Case 4: $v = 1.5m/sec$, $\omega = -1rad/sec$

Fig. 24. Minimum and maximum velocities possible at different points along the reference trajectory for Base Speed $v = 1.5m/sec$

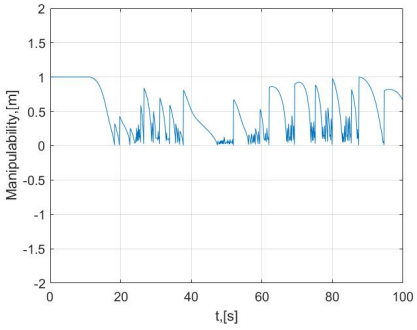

Fig. 25. Manipulability measures at the points considered along the reference trajectory for Base Speed $v = 1.5m/sec$

Tables VIII, IX, X and XI give the values of minimum and maximum possible ranges for the end effector velocity. Fig. 26 shows how the elongation of the manipulability ellipsoid which represents the minimum and maximum possible velocity ranges for the end effector is altered by moving forward. Increased linear velocity affects the elongation of the manipulability ellipsoid. High dexterity in all directions is necessary for tasks requiring intricate movements, such as maintenance or part assembly in small places, which favors a less elongated ellipsoid. Here, case 1 with the base speed $v = 1.5m/sec$, $\omega = -1rad/sec$ gives low values for manipulability ellipsoid elongation. It is also clear that the manipulability metric gets more complicated when the mobile manipulator is moving with a larger linear velocity. Both the combined impacts of the angular and linear motions are reflected in the manipulability ellipsoid.

TABLE VIII. MINIMUM AND MAXIMUM VELOCITY RANGES POSSIBLE FOR BASE SPEED $v = 0.2m/sec$

Maximum Range	Minimum Range
1.3986	0.1043
1.3868	0.1497
1.3516	0.2611
1.0491	0.4339
0.8123	0.4495
0.6363	0.3104
1.0809	0.2571
1.3528	0.2313
1.3480	0.2917

TABLE IX. MINIMUM AND MAXIMUM VELOCITY RANGES POSSIBLE FOR BASE SPEED $v = 1m/sec$

Maximum Range	Minimum Range
1.3914	0.1785
1.3529	0.2469
1.3449	0.2171
1.3800	0.1796
1.3904	0.1371
1.1687	0.3575
1.1948	0.3274
1.3792	0.1988
1.3334	0.2774

TABLE X. MINIMUM AND MAXIMUM VELOCITY RANGES POSSIBLE FOR BASE SPEED $v = 2m/sec$

Maximum Range	Minimum Range
1.3823	0.2018
1.3741	0.1835
1.3986	0.1327
1.3013	0.2712
1.3540	0.2537
1.3879	0.1848
1.1646	0.3455
1.3206	0.2328
1.3995	0.1455

IV. KINEMATIC CONTROL OF MM USING THE DATA OBTAINED FROM QUANTITATIVE ANALYSIS OF DESIGN CONSIDERATIONS

In this section, a kinematic controller is designed using the data obtained from a quantitative analysis of design considerations. When the MM is being controlled kinematically, its kinematic model is used to plan and direct the motion of the robot's end-effector in the workspace. Kinematic control seeks

to produce the desired end-effector movements and tasks while considering the robot's kinematic restrictions by computing the velocities of the movable base and the manipulator's joint angles.

TABLE XI. MINIMUM AND MAXIMUM VELOCITY RANGES POSSIBLE FOR BASE SPEED $v = 1.5m/sec$

Maximum Range	Minimum Range
1.3994	0.0885
1.3984	0.0252
1.3967	0.1152
1.3994	0.0111
1.3737	0.1060
1.0962	0.3423
1.3989	0.0037
1.2859	0.2709
1.3307	0.1841

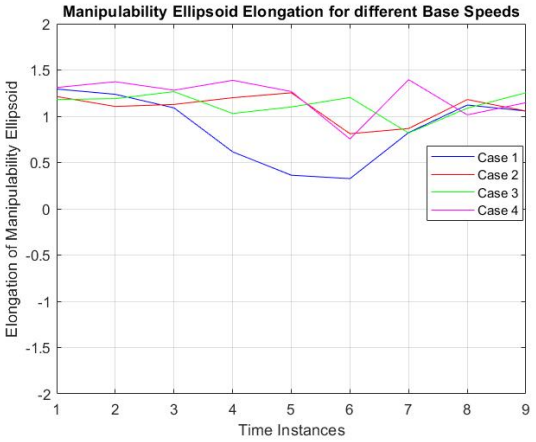

Fig. 26. Elongation of Manipulability ellipsoid for different base speeds

In Kinematic control, let the desired end effector positions and velocities be:

$$p_{arm_d} = \begin{bmatrix} x_{ee_d} & y_{ee_d} & z_{ee_d} \end{bmatrix} \tag{21}$$

$$\dot{p}_{arm_d} = \begin{bmatrix} \dot{x}_{ee_d} & \dot{y}_{ee_d} & \dot{z}_{ee_d} \end{bmatrix} \tag{22}$$

The actual end effector position and velocities available from sensors are:

$$p_{arm_{act}} = \begin{bmatrix} x_{ee_{act}} & y_{ee_{act}} & z_{ee_{act}} \end{bmatrix} \tag{23}$$

$$\dot{p}_{arm_{act}} = \begin{bmatrix} \dot{x}_{ee_{act}} & \dot{y}_{ee_{act}} & \dot{z}_{ee_{act}} \end{bmatrix} \tag{24}$$

The pseudo-inverse $J^{\#}$ of the combined Jacobian matrix J, given in (14) of the 6 DoF MM which is used for the controller design is given as:

$$J^{\#} = J^T (J J^T)^{-1} \tag{25}$$

From (13), the joint and the wheel velocities necessary to produce the proper end-effector motion can be determined from the differential kinematic model as follows:

$$\dot{q} = J^{\#} \begin{bmatrix} \dot{x}_{ee_d} \\ \dot{y}_{ee_d} \\ \dot{z}_{ee_d} \end{bmatrix} \tag{26}$$

The objective of the kinematic controller is to determine the control input $\dot{q}(t)$, which are the joint and wheel velocities so that the end effector follows the required trajectory. The controller is designed in such a way that the system is asymptotically stable as $t \to \infty$, $p_{arm_d} \to p_{arm_{act}}$, or as $t \to \infty$, $\tilde{p}_{arm} \to 0$ where $\tilde{p}_{arm} = p_{arm_d} - p_{arm_{act}}$, error in the end effector position. Error dynamics will be stable if:

$$\dot{\tilde{p}}_{arm} + K\tilde{p}_{arm} = 0 \tag{27}$$

where $K > 0$.

Substituting for $\dot{\tilde{p}}_{arm}$ and $\tilde{p}_{arm}$ the control law is:

$$\dot{q} = J^{\#}[\dot{p}_{arm_d} + K\tilde{p}_{arm}] \tag{28}$$

The block diagram representation of the kinematic controller of the MM is as given in Fig. 27:

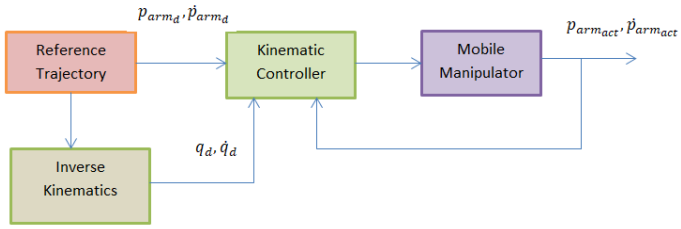

Fig. 27. Block Diagram of Kinematic Controller of MM

A. Simulation of Kinematic Controller Based on the Analysis of Performance Measures

To evaluate the kinematic controller's ability to follow the provided reference trajectory to the end effector, a MATLAB simulation for the 6 DoF MM is created. In this simulation, a circular trajectory is utilized to assess the controller's efficiency and performance. From Fig. 28, it is evident that the end effector is more accurately following the desired trajectory when the kinematic controller is applied to the MM with the selected link length ratio. The error graphs are shown in Fig. 29. Even though the error is high at the time, t=0, it reduces to a lower value within 0.5msec and remains within an error band of 0.01m during the entire time of operation. Fig. 30 illustrates the manipulability measures throughout the operation, and it is clear that the values are kept at a high level throughout.

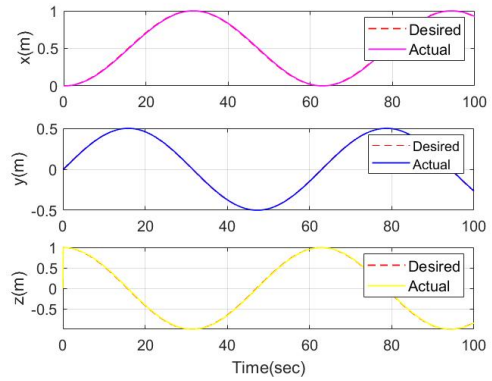

Fig. 28. Desired and actual x, y and z profiles of the end effector

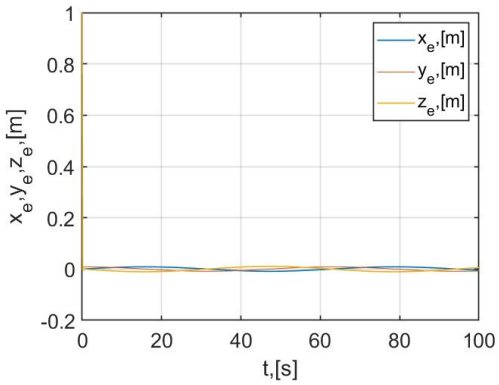

Fig. 29. Error profiles of end effector trajectory in x, y, and z directions

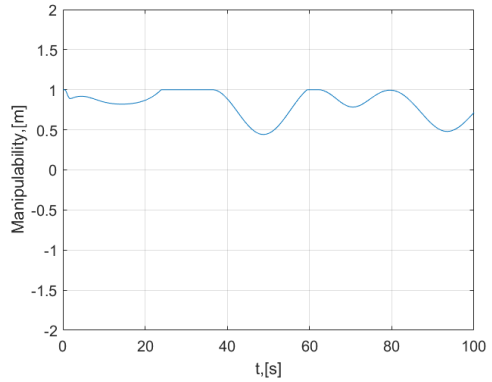

Fig. 30. Manipulability of the MM while following the reference trajectory

V. Conclusions

An organized kinematic analysis of design factors for an MM with six degrees of freedom is proposed in this paper. The study focuses on how the manipulability of the system is affected by the link length ratio and the mounting locations of the arm and mobile base. The objective was to identify the optimal values for these design parameters that maximize the manipulability of the mobile manipulator. The manipulator's maneuverability and capacity to reach various locations are greatly influenced by the link length ratios. Through a systematic variation of these ratios, significant shifts in the manipulability of the system was observed. Comprehensive simulations were used to determine the ideal link length ratio, which guarantees the manipulator a wide range of motion and flexibility while maintaining maximum manipulability. The effect of various mounting positions of the arm and base speed on manipulability was simulated. The optimal mounting position and base speed that gives maximum manipulability was chosen. Using the identified optimal design parameters values, a kinematic controller is designed and the MM is controlled to track a circular reference trajectory. This design considerations study is crucial for comprehending how the robotic system behaves when carrying out coordinated activities. The kinematic controller designed with the selected link length ratio and mounting position gives good results with very little tracking error for the end effector. As a future work, this analysis can be extended for any redundant MM for a specific application. Even though in this work, a kinematic controller is used, trajectory tracking can be done using various controllers applicable for varying payloads.

Acknowledgment

The author would like to thank APJ Abdul Kalam Technological University, Kerala, India

References

[1] C. C. Kemp, A. Edsinger, H. M. Clever and B. Matulevich, "The Design of Stretch: A Compact, Lightweight Mobile Manipulator for Indoor Human Environments," *2022 International Conference on Robotics and Automation (ICRA)*, pp. 3150-3157, 2022, doi: 10.1109/ICRA46639.2022.9811922.

[2] C. Wu, H. Fang, Q. Yang, X. Zeng, Y. Wei and J. Chen, "Distributed Cooperative Control of Redundant Mobile Manipulators With Safety Constraints," in *IEEE Transactions on Cybernetics*, vol. 53, no. 2, pp. 1195-1207, 2023, doi: 10.1109/TCYB.2021.3104044.

[3] Y. Zeng *et al*., "Task Sensing and Adaptive Control for Mobile Manipulator in Indoor Painting Application," in *IEEE/ASME Transactions on Mechatronics*, vol. 29, no. 4, pp. 2956-2963, 2024, doi: 10.1109/TMECH.2024.3399787.

[4] C. Liu, W. Feng, X. Shi, L. Song and Y. Liu, "Hierarchical Planning Algorithm for Redundant Mobile Manipulators to Follow a Given Trajectory," *2021 IEEE 11th Annual International Conference on CYBER Technology in Automation, Control, and Intelligent Systems (CYBER)*, pp. 122-127, 2021, doi: 10.1109/CYBER53097.2021.9588312.

[5] Y. S. Choi, I. Rhee, P. T. Hoang, and H. R. Choi, "Simple desired manipulability ellipsoid with velocity and force for control of redundant manipulator," *Journal of Mechanical Science and Technology*, vol. 37, no. 4, pp. 2033-2041, 2023, doi: 10.1007/s12206-023-0339-3.

[6] X. Yang, Z. Zhao, B. Ma, Z. Xu, J. Zhao and H. Liu, "Kinematic and Dynamic Manipulability Optimizations of Redundant Manipulators Based on RNN Model," in *IEEE Transactions on Industrial Informatics*, vol. 20, no. 4, pp. 5763-5773, 2024, doi: 10.1109/TII.2023.3334305.

[7] X. Li, L. Luo, H. Zhao, D. Ge, and H. Ding, "Inverse Kinematics Solution Based on Redundancy Modeling and Desired Behaviors Optimization for Dual Mobile Manipulators," *Journal of Intelligent and Robotic Systems*, vol. 108, no. 37, 2023, doi: 10.1007/s10846-023-01884-5.

[8] Y. Zhang, X. Yan, D. Chen, D. Guo, and W. Li, "QP-based refined manipulability-maximizing scheme for coordinated motion planning and control of physically constrained wheeled mobile redundant manipulators," *Nonlinear Dynamics*, vol. 85, pp. 245–261, 2016, doi: 10.1007/s11071-016-2681-9.

[9] I. Akli, "Trajectory planning for mobile manipulators including Manipulability Percentage Index," *International Journal of Intelligent Robotics and Applications*, vol. 5, pp. 543–557, 2021, doi: 10.1007/s41315-021-00190-3.

[10] F. Chen, M. Selvaggio and D. G. Caldwell, "Dexterous Grasping by Manipulability Selection for Mobile Manipulator With Visual Guidance," in *IEEE Transactions on Industrial Informatics*, vol. 15, no. 2, pp. 1202-1210, 2019, doi: 10.1109/TII.2018.2879426.

[11] A. Xie, T. Chen, G. Zhang, Y. Li and X. Rong, "Manipulability Enhancement of Legged Manipulators by Adaptive Motion Distribution," in *IEEE Transactions on Industrial Electronics*, vol. 72, no. 1, pp. 724-733, 2025, doi: 10.1109/TIE.2024.3413833.

[12] J. Leoro, and T. Hsiao, "Motion planning of nonholonomic mobile manipulators with manipulability maximization considering joints physical constraints and self-collision avoidance," *Applied Sciences*, vol. 11, no. 14, 2021, doi: 10.3390/app11146509.

[13] J. H. Choi, U. H. Sagong, J. H. Park, M. Kim and M. J. Hwang, "Motion Planning of Mobile Manipulator Using Virtual Impedance Energy Field," in *IEEE Access*, vol. 12, pp. 89776-89793, 2024, doi: 10.1109/ACCESS.2024.3400854.

[14] J. H. Choi, U. H. Sagong, J. H. Park, M. Kim and M. J. Hwang, "Motion Planning of Mobile Manipulator Using Virtual Impedance Energy Field," in *IEEE Access*, vol. 12, pp. 89776-89793, 2024, doi: 10.1109/ACCESS.2024.3400854.

[15] T. Pardi, V. Maddali, V. Ortenzi, R. Stolkin and N. Marturi, "Path planning for mobile manipulator robots under non-holonomic and task constraints," *2020 IEEE/RSJ International Conference on Intelligent Robots and Systems (IROS)*, pp. 6749-6756, 2020, doi: 10.1109/IROS45743.2020.9340760.

[16] J. H. Choi, U. H. Sagong, J. H. Park, M. Kim and M. J. Hwang, "Motion Planning of Mobile Manipulator Using Virtual Impedance Energy Field," in *IEEE Access*, vol. 12, pp. 89776-89793, 2024, doi: 10.1109/ACCESS.2024.3400854.

[17] I. Akli, "Trajectory planning for mobile manipulators including Manipulability Percentage Index," *International Journal of Intelligent Robotics and Applications*, vol. 5, pp. 543-557, 2021, doi: 10.1007/s41315-021-00190-3.

[18] F. Marić, O. Limoyo, L. Petrović, T. Ablett, I. Petrović and J. Kelly, "Fast Manipulability Maximization Using Continuous-Time Trajectory optimization," *2019 IEEE/RSJ International Conference on Intelligent Robots and Systems (IROS)*, pp. 8258-8264, 2019, doi: 10.1109/IROS40897.2019.8968441.

[19] J. Pankert and M. Hutter, "Perceptive Model Predictive Control for Continuous Mobile Manipulation," in *IEEE Robotics and Automation Letters*, vol. 5, no. 4, pp. 6177-6184, 2020, doi: 10.1109/LRA.2020.3010721.

[20] Y. Yang, Y. Yan, C. Hua and J. Li, "A Novel Predefined-Performance Control for Uncertain Nonholonomic Mobile Manipulator," in *IEEE Transactions on Industrial Informatics*, vol. 20, no. 4, pp. 6467-6476, 2024, doi: 10.1109/TII.2023.3345463.

[21] H. Zhang *et al*., "A novel coordinated motion planner based on capability map for autonomous mobile manipulator," *Robotics and autonomous systems*, vol. 129, 2020, doi: 10.1016/j.robot.2020.103554.

[22] H. Zhang, Q. Sheng, J. Hu, X. Sheng, Z. Xiong and X. Zhu, "Cooperative Transportation With Mobile Manipulator: A Capability Map-Based Framework for Physical Human–Robot Collaboration," in *IEEE/ASME Transactions on Mechatronics*, vol. 27, no. 6, pp. 4396-4405, 2022, doi: 10.1109/TMECH.2022.3155601.

[23] Li, Mantian, Zeguo Yang, Fusheng Zha, Xin Wang, Pengfei Wang, Ping Li, Qinyuan Ren, and Fei Chen. "Design and analysis of a whole-body controller for a velocity controlled robot mobile manipulator." Science China Information Sciences 63 (2020): 1-15.

[24] W. Yuan, Y. -H. Liu, C. -Y. Su and F. Zhao, "Whole-Body Control of an Autonomous Mobile Manipulator Using Model Predictive Control and Adaptive Fuzzy Technique," in *IEEE Transactions on Fuzzy Systems*, vol. 31, no. 3, pp. 799-809, 2023, doi: 10.1109/TFUZZ.2022.3189808.

[25] B. Bayle, J. Y. Fourquet, and M. Renaud, "Manipulability of wheeled mobile manipulators: Application to motion generation," *The International Journal of Robotics Research*, vol. 22, pp. 565-581, 2003, doi: 10.1177/02783649030227007.

[26] J. Fu, Y. Li, S. Yin, B. Zheng and J. Yuan, "Robust Anti-Disturbance Coordinated Control for Multiple Manipulators," in *IEEE Access*, vol. 8, pp. 95897-95905, 2020, doi: 10.1109/ACCESS.2020.2995770.

[27] M. Ou, H. Sun, Z. Zhang, and S. Gu, "Fixed-time trajectory tracking control for nonholonomic mobile robot based on visual servoing," *Nonlinear Dynamics*, vol. 108, pp. 251-263, 2022, doi: 10.1007/s11071-021-07191-8.

[28] Z. Xie, L. Jin, X. Luo, M. Zhou and Y. Zheng, "A Biobjective Scheme for Kinematic Control of Mobile Robotic Arms With Manipulability Optimization," in *IEEE/ASME Transactions on Mechatronics*, vol. 29, no. 2, pp. 1534-1545, 2024, doi: 10.1109/TMECH.2023.3313516.

[29] B. Bayle, M. Renaud, and J. Y. Fourquet, "Nonholonomic mobile manipulators: kinematics, velocities and redundancies," *Journal of Intelligent and Robotic Systems*, vol. 36, pp. 45-63, 2003, doi: 10.1023/A:1022361914123.

[30] O. M. Kapustina and A. I. Kobrin, "Research on Mobile Manipulators Singular Kinematics by Computer Algebra Systems," *2020 V International Conference on Information Technologies in Engineering Education (Inforino)*, pp. 1-4, 2020, doi: 10.1109/Inforino48376.2020.9111727.

[31] F. Zhou, F. Nie, T. An, B. Ma, and Y. Li, "Decentralized fault tolerant control of modular manipulators system based on adaptive dynamic programming," *International Journal of Control, Automation and Systems*, vol. 20, pp. 3252–3263, 2022, doi: 10.1007/s12555-021-0120-2.

[32] G. R. Petrović and J. Mattila, "Analytic Solutions for Wheeled Mobile Manipulator Supporting Forces," in *IEEE Access*, vol. 10, pp. 43235-43255, 2022, doi: 10.1109/ACCESS.2022.3169766.

[33] Huang, Qiang, Kazuo Tanie, and Shigeki Sugano. "Coordinated motion planning for a mobile manipulator considering stability and manipulation," *The International Journal of Robotics Research*, vol. 19, no. 8, pp. 732-742, 2000, doi: 10.1177/02783640022067139.

[34] N. Tan, Z. Zhu and P. Yu, "Neural-Network-Based Control of Wheeled Mobile Manipulators With Unknown Kinematic Models," *2020 International Symposium on Autonomous Systems (ISAS)*, pp. 212-216, 2020, doi: 10.1109/ISAS49493.2020.9378850.

[35] S. Liu *et al*., "Contact Force/Motion Hybrid Control for a Hydraulic Legged Mobile Manipulator via a Force-Controlled Floating Base," in *IEEE/ASME Transactions on Mechatronics*, vol. 29, no. 3, pp. 2316-2326, 2024, doi: 10.1109/TMECH.2023.3323541.

[36] C. W. Chang, C. W. Tao, "Design of a fuzzy trajectory tracking controller for a mobile manipulator system", *Soft Computing*, vol. 28, pp. 5197–5211, 2024, doi: 10.1007/s00500-023-09298-z.

[37] R. Ruchika, N. Kumar, "Force/position Control of Constrained Mobile Manipulators with Fast Terminal Sliding Mode Control and Neural Network," *Journal of Control, Automation and Electrical Systems*, vol. 34, pp. 1145–1158, 2023, doi: 10.1007/s40313-023-01032-2.

[38] J. Liao, F. Huang, Z. Chen, and B. Yao, "Optimization-based motion planning of mobile manipulator with high degree of kinematic redundancy," *International Journal of Intelligent Robotics and Applications*, vol. 3, pp. 115-130, 2019, doi: 10.1007/s41315-019-00090-7.

[39] Z. Li, L. Ma, Z. Meng, J. Zhang, and Y. Yin, "Improved sliding mode control for mobile manipulators based on an adaptive neural network," *Journal of Mechanical Science and Technology*, vol. 37, no. 5, pp. 2569-2580, 2023, doi: 10.1007/s12206-023-0432-7.

[40] K. Misawa, F. Xu, K. Sekiguchi, and K. Nonaka, "Model predictive

control for mobile manipulators considering the mobility range and accuracy of each mechanism," *Artificial Life and Robotics*, vol. 27, no. 4, pp. 855-866, 2022, doi: 10.1007/s10015-022-00799-y.

[41] M. Yu, X. Chen, Y. Qiu, C. Xing and P. Xu, "Nonlinear MPC based Whole-body Control for Mobile Manipulation," *2024 36th Chinese Control and Decision Conference (CCDC)*, pp. 5273-5278, 2024, doi: 10.1109/CCDC62350.2024.10588007.

[42] J. Bai, J. Du, T. Li, and Y. Chen, "Trajectory tracking control for wheeled mobile robots with kinematic parameter uncertainty," *International Journal of Control, Automation and Systems*, vol. 20, no. 5, pp. 1632-1639, 2022, doi: 10.1007/s12555-021-0212-z.

[43] D. P. Pagnotta, A. Monteriù, A. Freddi, S. Longhi, and A. Maciejewski, "Redundancy Resolution Scheme for Manipulators Subject to Inequality Constraints," *International Journal of Control, Automation and Systems*, vol. 21, no. 2, pp. 575-590, 2023, doi: 10.1007/s12555-021-0641-8.

[44] M. Rani, N. Kumar, and H. P. Singh, "Force/motion control of constrained mobile manipulators including actuator dynamics," *International Journal of Dynamics and Control*, vol. 7, pp. 940–954, 2019, doi: 10.1007/s40435-019-00523-y.

[45] H. Xing, A. Torabi, L. Ding, H. Gao, Z. Deng and M. Tavakoli, "Enhancement of Force Exertion Capability of a Mobile Manipulator by Kinematic Reconfiguration," in *IEEE Robotics and Automation Letters*, vol. 5, no. 4, pp. 5842-5849, 2020, doi: 10.1109/LRA.2020.3010218.

[46] T. Watanabe, "Effect of torque-velocity relationship on manipulability for robot manipulators," *Journal Mechanisms Robotics*, vol. 3, no. 4, pp. 1–9, 2011, doi: 10.1115/1.4004895.

[47] K. Nagatani, T. Hirayama, A. Gofuku and Y. Tanaka, "Motion planning for mobile manipulator with keeping manipulability," *IEEE/RSJ International Conference on Intelligent Robots and Systems*, vol. 2, pp. 1663-1668, 2002, doi: 10.1109/IRDS.2002.1043994.

[48] H. Bildstein, A. Durand-Petiteville and V. Cadenat, "Enhanced Visual Predictive Control Scheme for Mobile Manipulator," *2023 European Conference on Mobile Robots (ECMR)*, pp. 1-7, 2023, doi: 10.1109/ECMR59166.2023.10256320.

[49] V. Rayankula and P. M. Pathak, "Fault tolerant control and reconfiguration of mobile manipulator," *Journal of Intelligent and Robotic Systems*, vol. 101, no. 34, 2021, doi: 10.1007/s10846-021-01317-1.

[50] P. H. Chang, *Analysis and control of robot manipulators with kinematic redundancy*, MIT Artificial Intelligence Laboratory, 1987.

[51] P. S. Donelan, "Singularities of robot manipulators," *Singularity Theory*, pp. 189-217, 2007, doi: 10.1142/9789812707499_0006.

[52] N. Chen, F. Song, G. Li, X. Sun, and C. Ai, "An adaptive sliding mode backstepping control for the mobile manipulator with nonholonomic constraints," *Communications in Nonlinear Science and Numerical Simulation*, vol. 18, no. 10, pp. 2885-2899, 2013, doi: 10.1016/j.cnsns.2013.02.002.

[53] F. Chen, M. Selvaggio and D. G. Caldwell, "Dexterous Grasping by Manipulability Selection for Mobile Manipulator With Visual Guidance," in *IEEE Transactions on Industrial Informatics*, vol. 15, no. 2, pp. 1202-1210, 2019, doi: 10.1109/TII.2018.2879426.

[54] Y. Liu, Z. Li, H. Su, L. Jiang and C. -y. Su, "Whole Body Control of an Autonomous Mobile Manipulator Using Series Elastic Actuators," in *IEEE/ASME Transactions on Mechatronics*, 2021, doi: 10.1109/TMECH.2021.3057098.

[55] K. Jang, S. Kim and J. Park, "Motion Planning of Mobile Manipulator for Navigation Including Door Traversal," in *IEEE Robotics and Automation Letters*, vol. 8, no. 7, pp. 4147-4154, 2023, doi: 10.1109/LRA.2023.3279612.

[56] Y. Wan, J. Sun, C. Peers, J. Humphreys, D. Kanoulas and C. Zhou, "Performance and Usability Evaluation Scheme for Mobile Manipulator Teleoperation," in *IEEE Transactions on Human-Machine Systems*, vol. 53, no. 5, pp. 844-854, 2023, doi: 10.1109/THMS.2023.3289628.

[57] S. Thakar, P. Rajendran, A. M. Kabir and S. K. Gupta, "Manipulator Motion Planning for Part Pickup and Transport Operations From a Moving Base," in *IEEE Transactions on Automation Science and Engineering*, vol. 19, no. 1, pp. 191-206, 2022, doi: 10.1109/TASE.2020.3020050.

[58] J. Haviland, and P. Corke. "A purely-reactive manipulability-maximising motion controller," *arXiv*, 2002, doi: 10.48550/arXiv.2002.11901.

[59] R. Fareh, M. R. Saad, M. Saad, A. Brahmi, and M. Bettayeb, "Trajectory tracking and stability analysis for mobile manipulators based on decentralized control," *Robotica*, vol. 37, no. 10, pp. 1732-1749, 2019, doi: 10.1017/S0263574719000225.

[60] Z. Li and S. S. Ge. *Fundamentals in modeling and control of mobile manipulators*, vol. 49, 2013.

[61] T. Yoshikawa, "Manipulability of robotic mechanisms," *The international journal of Robotics Research*, vol. 4, no. 2, pp. 3-9, 1985, doi:10.1177/027836498500400201.

[62] N. Vahrenkamp, T. Asfour, G. Metta, G. Sandini and R. Dillmann, "Manipulability analysis," *2012 12th IEEE-RAS International Conference on Humanoid Robots (Humanoids 2012)*, pp. 568-573, 2012, doi: 10.1109/HUMANOIDS.2012.6651576.

[63] B. Bayle, J. -Y. Fourquet and M. Renaud, "Manipulability analysis for mobile manipulators," *Proceedings 2001 ICRA. IEEE International Conference on Robotics and Automation (Cat. No.01CH37164)*, vol.2, pp. 1251-1256, 2001, doi: 10.1109/ROBOT.2001.932782.

[64] T. Yoshikawa, "Manipulability and redundancy control of robotic mechanisms," *Proceedings. 1985 IEEE International Conference on Robotics and Automation*, pp. 1004-1009, 1985, doi: 10.1109/ROBOT.1985.1087283.

[65] J. F. Gardner and S. A. Velinsky, "Kinematics of mobile manipulators and implications for design," *Journal of Robotic Systems*, vol. 17, no. 6, pp. 309-320, 2000, doi: 10.1002/(SICI)1097-4563(200006)17:6¡309::AID-ROB2¿3.0.CO;2-9.